Brazilian Journal
of Chemical
Engineering

ISSN 0104-6632
Printed in Brazil
www.abeq.org.br/bjche

Vol. 36, No. 03, pp. 1289 - 1301, July - September, 2019
dx.doi.org/10.1590/0104-6632.20190363s20180423

NUMERICAL SIMULATION OF COAL GASIFICATION IN A CIRCULATING FLUIDIZED BED GASIFIER

Vikrant Sharma[1] and Vijay K. Agarwal[1*]

[1] Indian Institute of Technology Roorkee, Department of Chemical Engineering, Roorkee, Uttarakhand, India.
ORCID: 0000-0002-8628-7529; E-mail: vsharma@ch.iitr.ac.in - ORCID: 0000-0003-4328-4528

(Submitted: September 4, 2018 ; Revised: December 21, 2018 ; Accepted: April 1, 2019)

Abstract - This paper presents a 3D full-loop simulation of a circulating fluidized bed gasifier. The model is validated with experimental results from the literature. The validated model is thereupon used to compare Bubbling Fluidized Bed (BFB) and Circulating Fluidized Bed (CFB) gasifiers to highlight the effect of a change in fluidization regime from bubbling to fast fluidization on hydrodynamics, temperature and gas composition. Feed temperature as well as Air/Coal (A/C) and Steam/Coal (S/C) ratios are kept constant, whereas the velocity of the feed (Air-Steam) is increased so as to get into the fast fluidization regime. It was concluded that the flue gas from the CFB is richer in desired gases, i.e., CO and H_2 than that from BFB. H_2 remains approximately the same, CO_2 and CH_4 decreased to a negligible amount and CO approximately doubles when the regime is changed. In addition, tar content in the gas also decreases.
Keywords: Coal gasification; Bubbling fluidized bed; Circulating fluidized bed; Computational fluid dynamics; Full-loop simulation.

INTRODUCTION

Energy and a healthy environment are essential for humanity, societies and economies to develop and thrive. In 2016, the three most utilized fuels for energy production were crude oil, coal and natural gas with their respective shares of 33.28%, 28.11% and 24.13% in global energy consumption (BP, 2017). The supply of crude oil and natural gas is depleting and these fuels are not equitably distributed. In comparison, coal can last up to approximately three times longer. Furthermore, it is relatively cheaper, available from a wider variety of sources and has greater price stability (BP, 2017). Consequently, coal utilization is increasing rapidly, especially in China and India where strong economic growth and large populations are driving demand for energy. Coal is the most important fuel for electricity generation; approximately 40% and 70% of total generated electricity in the world and in India, respectively, is attributed to this fuel (IEA, 2017a). However, coal is the most carbon-intensive fuel which, in 2016, contributed the highest CO_2 emissions with 44.9% of total CO_2 emissions (IEA, 2017b). Hence, development of methods by which coal can be utilized in a clean, efficient, sustainable and cost-competitive way is the need of the hour.

Gasification offers the prospect of clean and efficient coal utilization to produce electricity in the Integrated Gasification Combined Cycle (IGCC), liquid fuels in Fischer-Tropsch (FT) Synthesis and a variety of chemicals (including hydrogen, ammonia, urea, methanol etc.) or combination of these (Poly-generation). Gasification offers an opportunity for both in-situ and pre-combustion carbon and sulphur capture, resulting in lower emissions. Furthermore, in the reducing and low temperature environment inside gasifiers, NH_3 and H_2S are produced instead of NO_x and SO_x. IGCC plants can achieve as much as 45 - 50% efficiency, thereby reducing carbon emissions.

* Corresponding author: Vikrant Sharma - E-mail: vsharma@ch.iitr.ac.in

There are a lot of gasifiers commercially available or in developmental stages. All of these gasifiers can be classified based on the state of solid movement (Moving-, Fluidized- and Entrained-bed), on the state of ash (Dry, Agglomerating and Slagging), on the state of coal feed (Dry, Slurry) and on the gasifier pressure (Atmospheric and Pressurized). Currently, a large spectrum of coals can be gasified and the main limitations exist for coals with low rank, high ash content and small particle size (Gräbner, 2015). Particularly coals from China or India contain high ash content (>30 wt%), ash fusion temperatures (>1600 °C) and sulphur content (>3 wt%) (Gräbner, 2015). As the ash content increases, many operational problems such as increased cost and fouling occur, along with a decrease in efficiency and conversion (Gräbner, 2015). India and China are the most coal importing countries, partially because of the fact that the high-ash coal abundant in these countries is difficult to utilize. Consequently, there is an increasing interest in the use of low-rank coals with high ash or moisture contents in emerging nations (e.g., India, Indonesia) (Gräbner, 2015).

Iyengar and Haque (1991) concluded that the high ash content in coal affects a moving bed gasification system the least, followed by bubbling and entrained bed gasification systems. Moving-bed gasifiers produce large amounts of tar and are unsuitable for large installations. In contrast, fluidized bed gasifiers have several advantages over other types of gasifiers such as: (1) better gas quality with moderate oxygen and steam consumption, (2) little fuel preparation, (3) high fuel flexibility, (4) potential for large capacities and scale-up (Gräbner, 2015). Hence, it was concluded that fluidized bed gasifiers are the most suitable for coal gasification of high ash Indian coals.

The fluidized bed gasifiers can be divided into bubbling fluidized bed (BFB) and circulating fluidized bed (CFB) gasifiers. The selection of a gasifier between these two types is the next step for the designers. The differences between BFB and CFB gasifiers have been discussed in literature (Basu, 2006), but a comprehensive assessment of the effect of this regime change is not presented until now. This paper is an attempt to fill that void by a three dimensional full-loop Computational Fluid Dynamic (CFD) simulation of a gasifier. The CFD models are proven to be an efficient, accurate and cost-effective tool to understand reactive fluidized bed systems. Li et al. (2014) concluded that full-loop simulation is required to accurately predict the transition between different fluidization regimes. Therefore, recent attempts (Liu, 2015; Liu, 2016; Yan, 2016; Liu, 2017; Kraft, 2017; Bogdanova, 2017; Shao, 2017; Yu, 2018) to study gasification are based on three dimensional full-loop CFD simulation. Therefore, the objective of this paper is to present a three-dimensional full-loop simulation of a CFB gasifier and compare it with the performance of a BFB gasifier to highlight the effect of regime change on various hydrodynamic, heat and mass transfer variables.

GOVERNING EQUATIONS

The Euler Granular Multiphase Model (EGMM) is utilized to simulate the CFB. In EGMM, gas and solid phases are assumed to be an inter-penetrating continuum and the rheological properties of the solid phase are calculated using Kinetic Theory of Granular Flow (KTGF). The governing equations of the gasifier include mass, momentum, energy and species transport equations for the gas and solid phases and a granular energy equation.

Mass and momentum conservation equations describe the hydrodynamics in the gasifier. The spatio-temporal distribution of density and volume fraction owing to interphase mass transfer (i.e., heterogeneous reactions) and convection is governed by the mass transport (continuity) equations for the solid and gas phases, which are as follows:

$$\frac{\partial\left(\rho_g\alpha_g\right)}{\partial t}+\nabla.\left(\rho_g\alpha_g u_g\right)=\sum R_s \tag{1}$$

$$\frac{\partial\left(\rho_s\alpha_s\right)}{\partial t}+\nabla.\left(\rho_s\alpha_s u_s\right)=-\sum R_s \tag{2}$$

where R_s is the volumetric rate of interphase mass transport, i.e., the rate of heterogeneous reactions in the case of gasifier.

The momentum conservation equations incorporate the effect of various external forces (such as pressure, shear, gravity) and interphase momentum transfer due to drag and mass transfer on the hydrodynamics. Thus, the momentum transport (Navier-Stokes) equations for the gas and solid phases are:

$$\frac{\partial\left(\rho_g\alpha_g u_g\right)}{\partial t}+\nabla.\left(\rho_g\alpha_g u_g u_g\right)=-\alpha_g\nabla P+\nabla.\tau_g+\alpha_g\rho_g g+K_{gs}\left(u_s-u_g\right)+\sum R_s u_s \tag{3}$$

$$\frac{\partial\left(\rho_s\alpha_s u_s\right)}{\partial t}+\nabla.\left(\rho_s\alpha_s u_s u_s\right)=-\alpha_s\nabla P-\nabla p_s+\nabla.\tau_s+\alpha_s\rho_s g+K_{gs}\left(u_g-u_s\right)-\sum R_s u_s \tag{4}$$

where τ_g and τ_s are shear stress tensors for the gas and solid phases, respectively, and are defined as (Johnson and Jackson, 1987):

$$\tau_g=\alpha_g\mu_g\left[\nabla u_g+\left(\nabla u_g\right)^T\right]+\alpha_g\left[\lambda_g-\frac{2}{3}\mu_g\right]\left(\nabla.u_g\right)I \tag{5}$$

$$\tau_s=\alpha_s\mu_s\left[\nabla u_s+\left(\nabla u_s\right)^T\right]+\alpha_s\left[\lambda_s-\frac{2}{3}\mu_s\right]\left(\nabla.u_s\right)I \tag{6}$$

The interphase momentum transfer coefficient (K_{gs}) depends on the drag force between solid particles and the gas phase and can be described by various correlations. Although drag models are not fully understood until now, the Energy-Minimization Multi-Scale (EMMS) (Zhang et al., 2008) model is currently considered to be the most effective model to describe the hydrodynamics of CFBs because it is derived from multi-scale analysis of mass and momentum conservation and the stability criterion based on a compromise between dominant mechanisms (i.e., gas tries to follow a path of least resistance and solid particles try to arrange themselves to minimize their potential energy). The EMMS model thus derived can be modelled according to the following scheme:

$$K_{gs} = \frac{3}{4} C_d \frac{\alpha_s \alpha_g \rho_g \left| u_s - u_g \right|}{d_s} \alpha_g^{-2.65} H_d \tag{7}$$

where the heterogeneity index Hd = $[A(Re+B)^C]/(H_{d,max})$ is calculated from the relative Reynolds Number Re = $(2\rho_g|u_g - u_s|d_s)/(\mu_g)$ and constants A, B and C which are dependent on voidage and are described as follows:

- for $0.448 < \alpha_g \leq 0.5$

$$\begin{cases} A = 0.7934 + 1.1175 e^{\left[-2\left(\frac{\alpha_g - 0.50778}{0.06956}\right)^2\right]} \\ B = 0 \\ C = 0 \end{cases} \tag{8}$$

- for $0.5 < \alpha_g \leq 0.6$

$$\begin{cases} A = 0.05204 + \dfrac{1.9743}{\left[1 + \left(\dfrac{\alpha_g}{0.53027}\right)^{50.25633}\right]} \\ B = 0.14294 - \dfrac{0.15047}{\left[1 + e^{\frac{-\alpha_g - 0.50084}{0.0047}}\right]} \left\{1 - \dfrac{1}{\left[1 + e^{\frac{-\alpha_g - 0.60902}{0.02736}}\right]}\right\} \\ C = 0.56038 - \dfrac{0.58092}{\left[1 + \left(\dfrac{\alpha_g}{0.54322}\right)^{34.39893}\right]} \end{cases} \tag{9}$$

- for $0.6 < \alpha_g \leq 0.98$

$$\begin{cases} A = \left(429.90532 - 434.69389\alpha_g\right)^{-0.5868} \\ B = \dfrac{\alpha_g - 1.02901}{-1.58454 + 7.56707\left(\alpha_g - 1.02901\right) - 19.64414\left(\alpha_g - 1.02901\right)^2} \\ C = \left(0.05377 - 0.05394\alpha_g\right)^{0.163018} \end{cases} \tag{10}$$

- nd for $0.98 < \alpha_g \leq 0.9997$

$$\begin{cases} A = 0.36777 + \dfrac{5.13409}{\left[1 + e^{\frac{-\alpha_g - 0.995945}{0.00447}}\right]} \left\{1 - \dfrac{1}{\left[1 + e^{\frac{-\alpha_g - 0.999915}{0.00044}}\right]}\right\} \\ B = 0.0175 + 0.71397 e^{\left[-0.5\left(\frac{\alpha_g - 0.9986}{0.00186}\right)^2\right]} \\ C = 0.32769 - 0.25491 e^{\left[-0.5\left(\frac{\alpha_g - 0.99863}{0.00969}\right)^2\right]} \end{cases} \tag{11}$$

$H_{d,max}$ is a constant whose value is equal to 3.04.

The bulk viscosity of the gas phase is identically zero and the properties of the solid phase, i.e., bulk viscosity (λ_S) (Lun et al., 1984), viscosity (μ_S) and solid pressure (p_S) (Lun et al., 1984) depend on granular temperature and can be quantified with the following correlations:

$$\lambda_s = \frac{4}{3} \alpha_s \rho_s d_s g_0 \left(1 + e_{ss}\right) \sqrt{\frac{\theta_s}{\pi}} \tag{12}$$

$$\mu_s = \frac{4}{5} \alpha_s \rho_s d_s g_0 \left(1 + e_{ss}\right) \sqrt{\frac{\theta_s}{\pi}} + \frac{10 \rho_s d_s \sqrt{\theta_s \pi}}{96 \alpha_s \left(1 + e_{ss}\right) g_0} \left[1 + \frac{4}{5} g_0 \alpha_s \left(1 + e_{ss}\right)\right]^2 + \frac{p_s \sin\varphi}{2\sqrt{I_{2D}}} \tag{13}$$

$$p_s = \alpha_s \rho_s \theta_s + 2\rho_s \left(1 + e_{ss}\right) \alpha_s^2 g_0 \theta_s \tag{14}$$

The solid viscosity contains three parts, i.e., collisional, kinetic and frictional. The Gidapow correlation (Gidaspow et al., 1992) is considered for the collisional and kinetic terms and, for frictional viscosity, Schaeffer's expression (Schaeffer, 1987) is taken in the present model. The granular temperature (θ_S), which quantifies the fluctuating energy of the solids, is calculated from the granular energy equation (Ding and Gidaspow, 1990):

$$\frac{3}{2}\left[\frac{\partial\left(\rho_s \alpha_s \theta_s\right)}{\partial t} + \nabla.\left(\rho_s \alpha_s \theta_s u_s\right)\right] = \left(-p_s I + \tau_s\right) : \nabla u_s + \nabla.\left(k_{\theta s} \nabla \theta_s\right) - \gamma_{\theta s} - 3K_{gs}\theta_s \tag{15}$$

where $k_{\theta S}$ and $\gamma_{\theta S}$ describe diffusive transport and collisional dissipation of granular energy, respectively, and are defined as follows (given by Gidaspow et al., 1992 and Lun et al., 1984, respectively):

$$k_{\theta s} = \frac{150\rho_s d_s\sqrt{\theta_s \pi}}{384(1+e_{ss})g_0}\left[1+\frac{6}{5}\alpha_s g_0 (1+e_{ss})\right]^2 + 2\rho_s \alpha_s^2 d_s (1+e_{ss}) g_0 \sqrt{\frac{\theta_s}{\pi}} \quad (16)$$

$$\gamma_{\theta s} = \frac{12\left(1-e_{ss}^2\right)g_0}{d_s\sqrt{\pi}}\rho_s \alpha_s^2 \theta_s^{3/2} \quad (17)$$

The radial distribution function (g_0) is used to counter the common problem of unphysical solid fraction encountered in TFM due to the artificial fluid behaviour of the solid phase and is given as (Ogawa et al., 1980):

$$g_0 = \left[1-\left(\frac{\alpha_s}{\alpha_{s,max}}\right)^{\frac{1}{3}}\right]^{-1} \quad (18)$$

where $\alpha_{s,max}$ = 0.63. Temperature of both gas and solid phases changes due to both heterogeneous and homogeneous reactions. In addition, convection and conduction within the phase, as well as interphase heat transfer, affect the temperature. The energy transport equations, which incorporate the aforementioned heat transfer mechanisms to quantify changes in temperature for the gas and solid phases, are given as:

$$\frac{\partial\left(\alpha_g \rho_g H_g\right)}{\partial t} + \nabla.\left(\alpha_g \rho_g H_g u_g\right) = \tau_g : \nabla u_g - \nabla.q_g + h\left(T_s - T_g\right) + \sum R_s \Delta H_{Rs} + \sum R_g \Delta H_{Rg} \quad (19)$$

$$\frac{\partial\left(\alpha_s \rho_s H_s\right)}{\partial t} + \nabla.\left(\alpha_s \rho_s H_s u_s\right) = \tau_s : \nabla u_s - \nabla.q_s + h\left(T_g - T_s\right) - \sum R_s \Delta H_{Rs} \quad (20)$$

where $H_g = \Sigma Y_i H_i$ and $H_S = C_S T_S$ are the enthalpies of the gas and solid phases respectively. Conductive transfer of heat in the gas and solid phases is governed by $q_g = k_g \nabla T_g$ and $q_S = k_S \nabla T_S$. Interphase transfer of heat by convection is denoted by the heat transfer coefficient (h) which is calculated with the Gunn (1978) correlation as follows:

$$h = \frac{6k\alpha_s \alpha_g Nu}{d_s^2} \quad (21)$$

$$Nu = \left(7-10\alpha_g+5\alpha_g^2\right)\left(1+0.7\,Re^{0.2}\,Pr^{\frac{1}{3}}\right) + \left(1.33-2.4\alpha_g+1.2\alpha_g^2\right)Re^{0.7}\,Pr^{\frac{1}{3}} \quad (22)$$

ΔH_{Rs} and ΔH_{Rg} are the heats of heterogeneous and homogeneous reactions, respectively.

Gas composition changes in the gasifier due to reactions, as well as due to diffusion and convection. Diffusion in the case solid species is considered to be zero. Therefore, the species transport equations describing the spatio-temporal distribution of various gas and solid species are given as:

$$\frac{\partial\left(\rho_g \alpha_g Y_{gi}\right)}{\partial t} + \nabla.\left(\rho_g \alpha_g u_g Y_{gi}\right) = \alpha_g \rho_g \nabla.\left[D_i \nabla Y_{gi}\right] + \sum R_{gi} + \sum R_{si} \quad (23)$$

$$\frac{\partial\left(\rho_s \alpha_s Y_{si}\right)}{\partial t} + \nabla.\left(\rho_s \alpha_s u_s Y_{si}\right) = \sum R_{si} \quad (24)$$

where D_i is the diffusivity of the i^{th} specie in the mixture.

Eight heterogeneous and eight homogeneous reactions are considered for the description of the gasification system, which are given in Table 1 along with their kinetic coefficients for extended Arrhenius equation, i.e., $k = AT^n \exp(-E/RT)$. The Kobayashi two-step model is used for devolitilization (Kobayashi et al., 1977) and the composition of the volatiles is calculated based on the ultimate and proximate analysis of the coal given in Table 2.

Furthermore, the equation of state (Ideal Gas equation) and volume fraction equation are also required to close the problem and are as follows:

$$PM = \rho_g R T_g \quad (25)$$

$$\alpha_g + \alpha_s = 1 \quad (26)$$

Thus, simultaneous solution of mass, momentum, energy and species conservation equations is carried out to predict the performance of the gasifier.

GEOMETRY

The geometry envisaged for the CFB loop of Ju et al. (2010) is given in Figure 1. The CFB loop consists of a riser, a cyclone and a return-pipe. The riser is a cylindrical vessel with diameter of 0.9 m and height of 12 m. Air or an air/steam mixture is blown from the inlet at the bottom to fluidize the particles in the riser. Xuzhou bituminous coal was used in the present study. Table 2 shows the basic characteristics of Xuzhou bituminous coal.

SIMULATION SET-UP

The commercial CFD software ANSYS Fluent® v.15 is used for the simulations. The simulation setup is given in Table 3. The properties not listed in Table 3 were retained at their default values. The EMMS Heterogeneity index, heterogeneous reaction rate and particle density were coupled with Fluent using

Table 1. Heterogeneous and homogeneous reaction kinetics.

S.No.	Reaction	A	E	n
	Heterogeneous Reactions			
1	Volatiles → 0.07CO + 0.01CO_2 + 0.03CH_4 + 0.03H_2 + 0.01H_2O + 0.013NH_3 + 0.0031H_2S + 0.056Tar	$A_1 = 2x10^5\ s^{-1}$ $A_2 = 1.3x10^7\ s^{-1}$	$E_1 = 104.6x10^3$ J/mol $E_2 = 167.4x10^3$ J/mol	0
2	Tar + O_2 → 0.05CO + 0.01CO_2 + 0.003H_2O	$2x10^5\ s^{-1}$	$104.6x10^3$ J/mol	0
3	Moisture → H_2O	$1.1x10^5\ s^{-1}$	88700.8 J/mol	
4	C + H_2O → CO + H_2	$5.95x10^{-5}\ Pa^{-1}s\text{-}1$	113486.1 J/mol	0
5	C + O_2 → CO_2	$1.5x10^6\ s^{-1}$	108730.5 J/mol	0
6	C + ½ O_2 → CO	$0.046\ atm^{-1}s^{-1}$	$110.5x10^3$ J/mol	0
7	C + CO_2 → 2CO	$3.92\ Pa^{-1}s^{-1}$	223871.08 J/mol	0
8	C + 2H_2 → CH_4	$8.36x10^{-4}\ atm^{-1}s^{-1}$	67160.5 J/mol	0
	Homogeneous Reactions			
9	CH_4 + H_2O → CO + 2H_2	$3.1x10^5\ m^3/mol.s$	124710 J/mol	0
10	CO + 3H_2 → CH_4 + H_2O	$1.1698x10^{10}\ (m^3/mol)^2s^{-1}$	$3.9824x10^5$ J/mol	0
11	CH_4 + 2O_2 → CO_2 + 2H_2O	$3.552x10^{11}\ K.m^3/mol.s$	$1.3053x10^5$ J/mol	-1
12	CH_4 + 3/2 O_2 → CO + 2H_2O	$5.102x10^{11}\ m^3/mol.s$	$2x10^5$ J/mol	0
13	CO + H_2O → CO_2 + H_2	$2.78\ m^3/mol.s$	$1.2567x10^4$ J/mol	0
14	CO_2 + H_2 → CO + H_2O	$104905.7\ m^3/mol.s$	$4.5448x10^4$ J/mol	0
15	CO + ½ O_2 → CO_2	$2.2x10^9\ (m^3/mol)^{0.25}s^{-1}$	$1.67x10^5$ J/mol	0
16	H_2 + ½ O_2 → H_2O	$5.159x10^{10}\ K^{1.5}(m^3/mol)^{1.5}s^{-1}$	$2.8517x10^4$ J/mol	-1.5

Table 2. Basic characteristics of Xuzhou bituminous coal.

Proximate Analysis (wt%)				Ultimate Analysis (Dry ash free, wt%)				
Char	**Volatiles**	**Moisture**	**Ash**	**C**	**H**	**O**	**N**	**S**
45.06	29.24	6.62	19.08	80.76	5.01	12.13	1.36	0.74

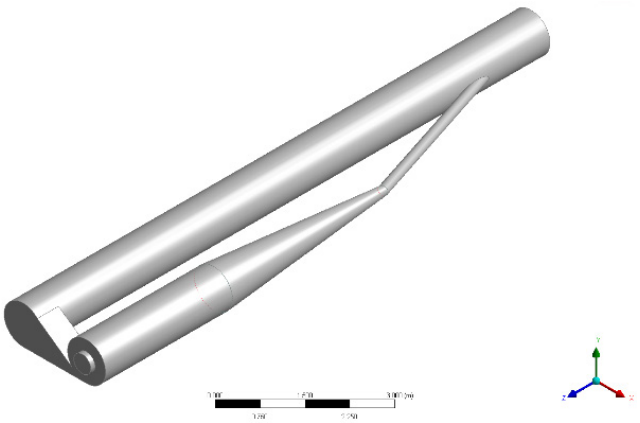

Figure 1. Geometry of the CFB loop.

DEFINE_EXCHANGE_PROPERTY, DEFINE_HET_RXN_RATE and DEFINE_PROPERTY User-Defined Function (UDF) macros, respectively. Ash was used as bed material, which filled up the riser up to a height of 300 mm initially, so it was patched in fluent with a minimum fluidization volume fraction of 0.552. Initial temperature of the bed is 1073 K and it is filled with air. After reaching a quasi-steady state, 2 s of data is time-averaged, and used in our analysis.

RESULTS AND DISCUSSION

This section presents a grid independence study, validation of the model and finally a comparison between BFB and CFB gasifiers based not only on hydrodynamic variables such as solid volume fraction, velocity of both solid and gas phases, static pressure, but also on temperature and composition of the product gas.

Grid independence

CFD models are solved on discretized grids by numerical methods. The meso-scale flow structures can only be captured with a relatively fine mesh. Since a coarse mesh can lead to false macroscopic flow fields, a grid independence study is necessary to evaluate the effect of grid resolution on the final solution. Considering these facts, three case studies with Coarse (40439 cells), Finer (106478 cells) and Finest (186987 cells) mesh were conducted to observe the effects of the mesh resolution on the simulation results. The instantaneous results of composition of the products at the outlet and axial profiles of gas and solid temperature, static pressure and solid volume fraction along the riser axis for the base case after 200 time-steps were compared and the results are shown in Figure 2. It should be noted that sometimes the mean value can show similar values when instantaneous values are different; that is why, for grid independence, instantaneous value are compared.

It can be observed from Figure 2(a) that the outlet gas composition is quite similar for all the three meshes. Figure 2(b), (c), (d) and (e) present reasonably similar axial profiles of solid volume fraction, static pressure and solid and gas temperature. Solid temperature (Figure 2(d)) shows the largest variation. Thus, it can be concluded that all the three meshes will provide reasonably accurate data. Keeping the aforementioned observations and the limitation on the execution time

Table 3. Simulation setup.

Solver	Pressure-based, Transient
Models	Laminar, Multiphase (Eulerian, 2 Phases), Energy, Species Transport (Volumetric reactions, Full multicomponent diffusion), Discrete Phase (Interaction with continuous phase, No tracking)
Materials and Phases	Fluid (Primary phase, Mixture of H_2O, O_2, N_2, CO, CO_2, CH_4, H_2, NH_3, H_2S and TAR (C_6H_6), Finite rate reactions - Homogeneous, Ideal gas), Coal (Secondary phase, Mixture of Char (C), Volatiles (coal-hv-volatiles), Moisture (H_2O(l)) and Ash (SiC), No reactions, Granular, Granular Temperature Model = Phase property, Diameter = $1x10^{-3}$ m, Density = 1400 kg/m^3 (UDF), Granular Viscosity = Gidaspow, Granular Bulk Viscosity = Lun et al., Frictional Viscosity = Schaeffer, Heat capacity = 1260 J/kg.K, Thermal Conductivity = 0.0454 W/m.K, Mass Diffusivity = 10^{-10} m^2/s for all components)
Phase Interaction	Drag = EMMS (Zhang et al., 2008): Wen-Yu (Drag Correction (UDF)), Heat = Gunn, Reactions - Heterogeneous (UDF)
Boundary Conditions	Inlet = Velocity Inlet [Base Case - (Primary phase = 1.16 m/s (Base Case), Composition = (79% N2, 21% O2), Temperature = 1073 K, Secondary phase = 0.0 m/s)] Outlet = Pressure Outlet (Gauge Pressure = 0.0) Coal Inlet = Mass Flow Inlet [Base Case - (Primary phase = 0.0 kg/s, Secondary phase = 0.34 kg/s, Volume fraction = 0.552, Composition = (45.06% Char, 29.24% Volatiles, 6.62% Moisture, 19.08% Ash))] Wall = Primary phase = No Slip, Secondary phase = Partial Slip (Johnson and Jackson, 1987) (Specularity Coefficient = 0.6)
Pressure Velocity Coupling	Phase-Coupled SIMPLE
Spatial Discretization	First order upwind
Temporal Discretization	First order implicit
Gradient	Least square cell based
Time Step	0.0001 s

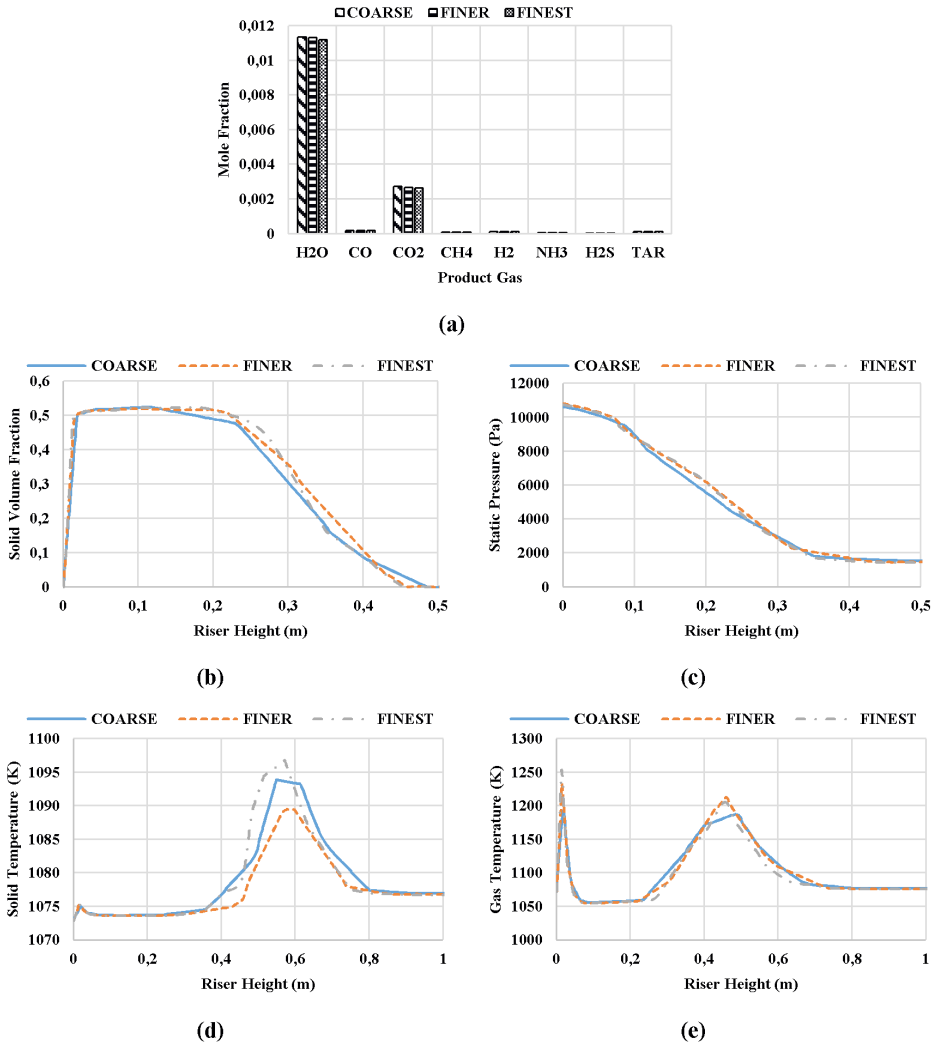

Figure 2. Grid independence study.

in consideration, the Coarse mesh was chosen for this study and is presented in Figure 3.

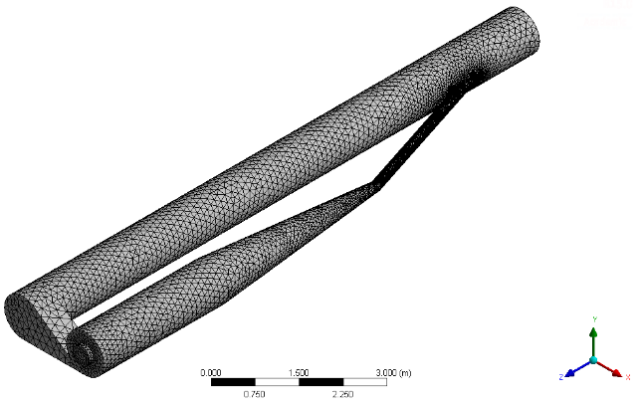

Figure 3. Mesh of the CFB loop.

Model validation

Table 4 shows comparison between experimental and simulation results for the mean outlet gas composition and mean bed temperature at steady state for A/C = 2.65; S/C = 0.0 (Base Case) and A/C = 2.65; S/C = 0.15 for the BFB. The relative error between the two measurements is also calculated to ensure the validity of the model. It can be seen from the two cases that the maximum normalized percentage error between the simulation and the experimental data is 7.98% for the variables tested, which is less than the engineering acceptable limit, i.e., 10%. Thus, it is concluded that the modelling and simulation work will be able to produce acceptable results.

Comparison between BFB and CFB coal gasification

Transient variation of the outlet gas temperature and outlet mixture mass flow rate of BFB and CFB gasifiers is given in Figure 4. It can be clearly seen from the graphs that, while the BFB gasifier reaches a quasi-steady state at around 8 seconds, the CFB gasifier takes longer to reach a reasonably stable region. Furthermore, the fluctuations in the profiles are comparatively more in the case of the CFB gasifier. Comparison between published results for a BFB gasifier (Armstrong et al., 2011) and CFB Gasifier (Zhang et al., 2015; Hassan, 2013) shows a similar trend. It should be noted that negative values of the outlet mass flow rate indicate that flow is going out.

Figure 5 presents a comparison between the axial distribution of mean static pressure along the axis of the riser for the BFB and the CFB gasifiers. From Figure 5, it can be stated that there is a large variation between the pressures of the two operations and pressure inside a CFB is significantly higher than in a BFB. While observing the total pressure drop in the riser, although the pressure drop in the CFB (1946.96 Pa) is larger than in a BFB (1489.585 Pa), it is not as large a deviation as we have seen in pressure. Afrooz et al. (2016) present an axial profile of pressure in a BFB and Lu et al. (2013) and Zhang et al. (2008) present it for a CFB similar to the ones presented here.

Axial variation of the solid volume fraction along the axis of the riser is given in Figure 6. It can be clearly seen from the figure that the bottom bed is quite dense in case of a BFB, while the rest of the riser is an empty freeboard region. In case of a CFB, almost the same value of solid volume fraction is observed throughout the riser with a very small increase in the lower part of the riser. From the zoomed view, it can be seen that the solid volume fraction in a CFB is always higher as compared to BFB except in the bed. The sudden increase in the solid volume fraction at the end of the

Table 4. Comparison between experiment and simulation.

	A/C = 2.65; S/C = 0.0			A/C = 2.65; S/C = 0.15		
	Experiment	**Simulation**	**Error (%)**	**Experiment**	**Simulation**	**Error (%)**
CO (mol%)	14.12	14.19	0.47	15.66	14.44	7.77
CO_2 (mol%)	11.04	11.92	7.98	11.19	11.98	7.05
CH_4 (mol%)	5.78	5.94	2.63	5.20	4.90	5.63
H_2 (mol%)	12.47	12.76	2.37	13.33	12.71	4.68
Bed Temperature (°C)	960.32	890.24	7.30			

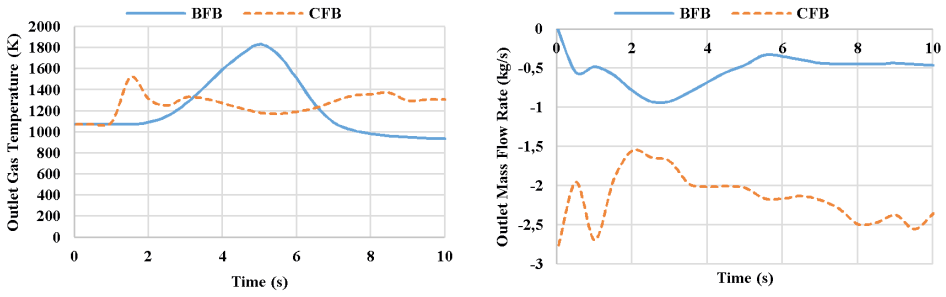

(a) **(b)**

Figure 4. Transient variation of (a) outlet gas temperature and (b) outlet mass flow rate.

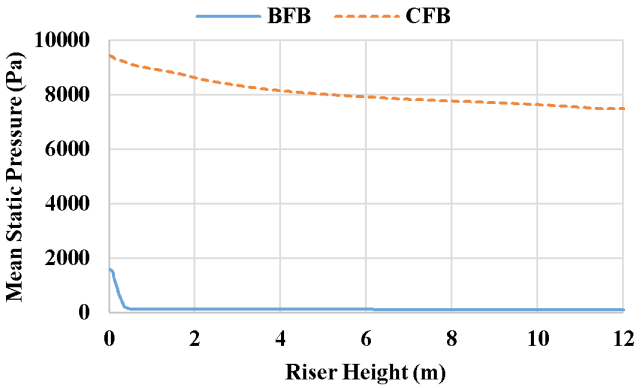

Figure 5. Axial distribution of mean static pressure along the riser axis.

riser is due to a cluster formation on the wall of the riser while gas is moving towards the exit and into the connector to the cyclone. Since the solid particles are distributed throughout the riser, in the case of a CFB, more pronounced gas solid contact and in turn better heat and mass transfer will be observed. In addition, in the case of CFB, heterogeneous reactions are not limited to the bed region.

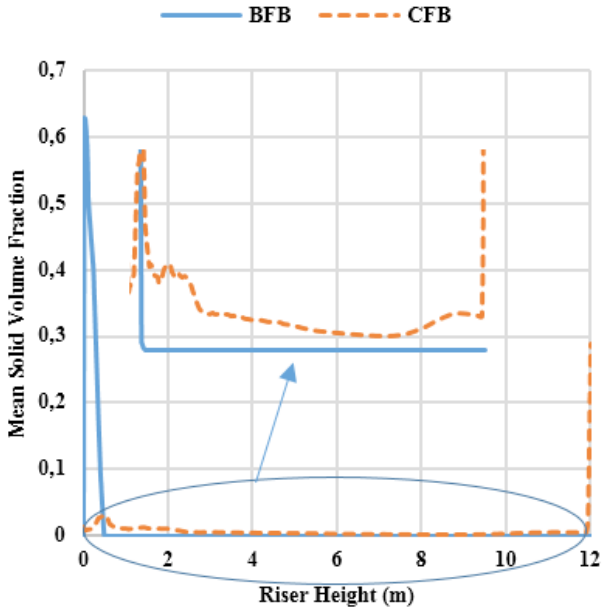

Figure 6. Axial distribution of mean solid volume fraction along the riser axis.

Radial distribution of the solid volume fraction at different riser heights is shown in Figure 7. It can be seen from Figure 7 that, at 0.1 m, the solid volume fraction in a BFB is very high in comparison to CFB; at 0.5 m similar values are obtained for both types and, at 1 m and beyond, the solid volume fraction in a BFB is constantly zero. In contrast, in the CFB at and after 1 m, the solid volume fraction is always higher than zero and it is high at the walls and relatively lower in the central region, i.e., typical core-annular flow is observed. Below 1 m, the recirculating gas and particles from the return leg push particles to other side and create a lot of turbulence. Figure 7(b) shows that the solid volume fraction decreases as riser height increases. Axial and radial profiles of the solid volume fraction in a BFB (Loha et al., 2012; Wang and Liu, 2010) and CFB (Zhang et al., 2008) corroborate the findings presented here.

Figure 8 shows radial profiles of the mean solid axial velocity at different riser heights. It can be clearly seen that, while CFB can be distinguished from characteristic core-annular flow, i.e., high axial velocities in the central region and low or even negative axial velocities near the wall, BFB shows negative mean velocities throughout the bed. Although bubbles, whose void fraction is close to one, push the particles while moving towards the freeboard region, on an average, the particle's tendency is to move

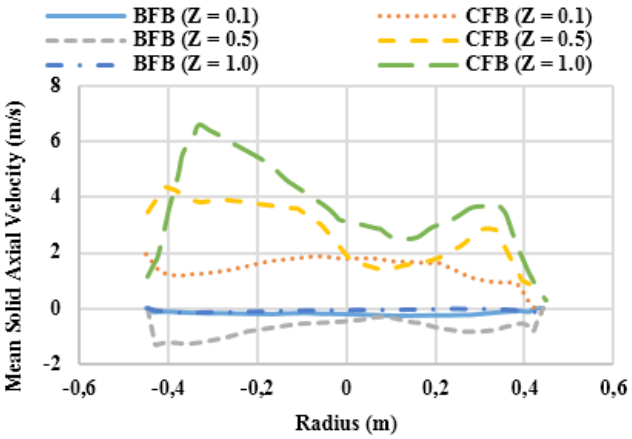

Figure 8. Radial distribution of mean solid axial velocity at various riser heights.

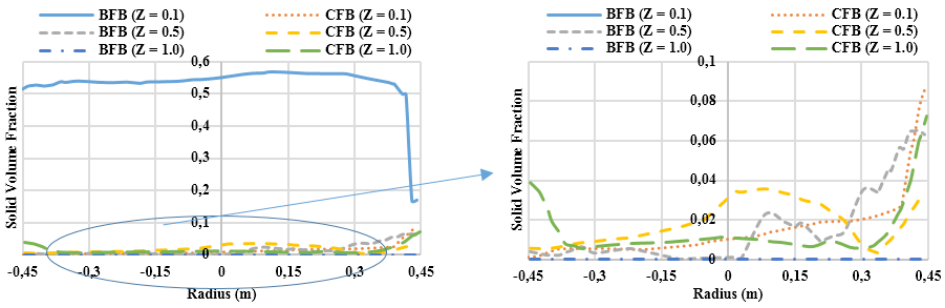

Figure 7. Radial distribution of mean solid volume fraction at various riser heights.

downwards under the effect of gravity. In addition, the gas and particles coming from coal and recycle inlets keep the axial velocity negative in the BFB, where the gas velocity is lower. At around 1 m, where the freeboard region starts, the velocity is close to zero and will remain the same throughout the riser. In contrast, CFB shows increasing velocities with increasing riser height. Zhao et al. (2015), Almuttahar et al. (2008), Zhang et al. (2001), Peng et al. (2016) and Gungor et al. (2007) show similar solid axial velocity profiles.

Figure 9 presents the radial distribution of mean gas axial velocities at different riser heights of BFB and CFB. It can be seen from the figure that mean gas axial velocities in the case of CFB are much higher than BFB. Also, they are much higher than the corresponding solid velocities. The sudden decrease at the centre of the riser at 0.5 and 1 m and in the near-wall region at 0.1 m can be attributed to high negative velocity gases coming from the return-pipe. Owing to the same reason, gas velocities near the wall at 0.5 and 1 m achieve exceptionally high values. After the effect of the return-pipe settles, mean gas velocities are approximately the same throughout the riser with core-annular structure.

Figure 10 shows the axial distribution of gas and solid temperatures in BFB and CFB along the riser axis. It can be observed from the figure that, in the case of the BFB, solid and gas temperatures almost exactly overlap each other; in contrast, in the case of CFB, difference between the solid and gas temperature is very high near the inlet and decreases along the riser height. The temperature of the solid is lower because only a fraction of the heat evolved during heterogeneous combustion reactions remains in the solids. The rest of the heat is carried out to the bulk gas phase by the product gases. In addition, the heat of homogeneous combustion reactions is entirely consumed by the gas phase. Moreover, the difference between gas and solid phase decreases along the riser due to interphase heat transfer. In both BFB and CFB,

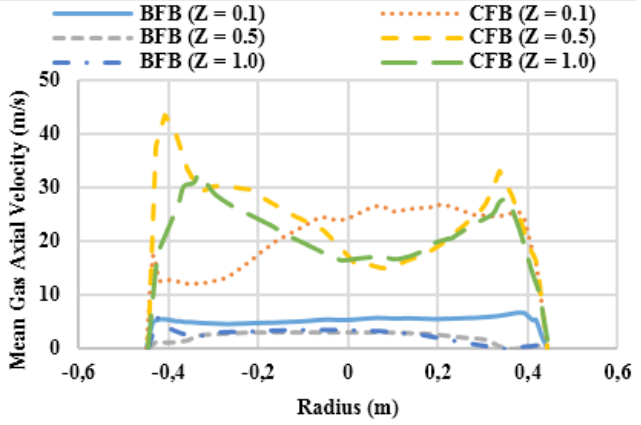

Figure 9. Radial distribution of mean gas axial velocity at various riser heights.

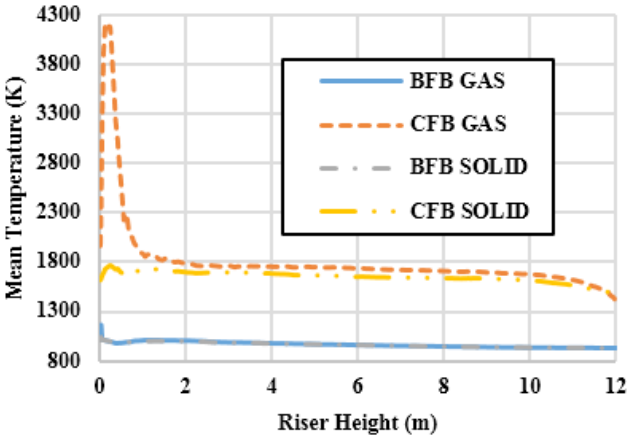

Figure 10. Axial profile of mean gas and solid temperature.

the temperature is almost uniform throughout the bed (slight decrease with increasing riser height due to endothermic gasification reactions) by virtue of the excellent heat transfer characteristics of the fluidized bed, except near the inlet. It is an expected outcome since, at the inlet, oxygen and coal are fed into the gasifier and the fastest and most exothermic of all the gasification reactions, the combustion reaction, takes place. Consequently, there is a huge temperature rise and almost complete elimination of oxygen at the inlet. Similar profiles of gas and solid temperatures for a CFB gasifier were observed in other studies (Hassan, 2013; Zhou et al., 2011; Wu et al., 2017). In case of a BFB, the highest gas, highest solid, lowest gas and lowest solid temperatures are 893.23, 775.73, 653.35 and 652.27 ºC respectively, whereas, in the case of CFB, these values are 3916.93, 1499.25, 1130.73 and 1127.51 ºC respectively.

Temperature in the BFB is well below the ash softening temperature (~1200 ºC); it should be increased up to this limit to maximize yield and efficiency. In contrast, in CFB, the temperatures of both gas and solid phases are higher than the ash softening limit at the current operating conditions. The higher temperature will give maximum conversion but operational difficulties of ash melting such as defluidization, corrosion etc. need to be overcome, especially when using high ash coals. For high ash coals, we need to avoid ash slagging. Furthermore, the assumption of kinetically controlled reactions is not valid beyond 1200 ºC, so the model has to be changed to include mass transfer resistances. The aforementioned purpose can be achieved by decreasing the inlet oxygen flow rate, thereby decreasing the combustion rate and heat release.

Figure 11 shows contours of the instantaneous mole fraction of different gas species in the BFB Gasifier at 10 s. Similarly, Figure 12 shows the same for the CFB gasifier. It was observed from the figures that the

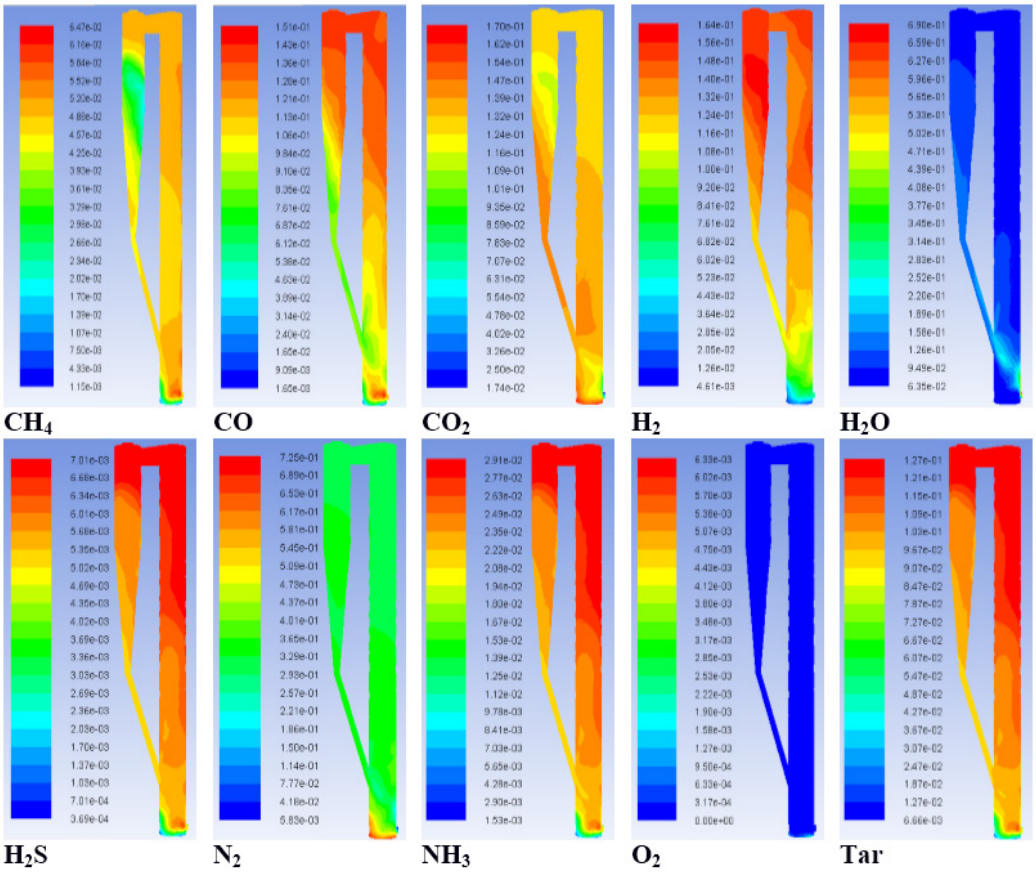

Figure 11. Contours of instantaneous species mole fraction at 10 sec in BFB gasifier.

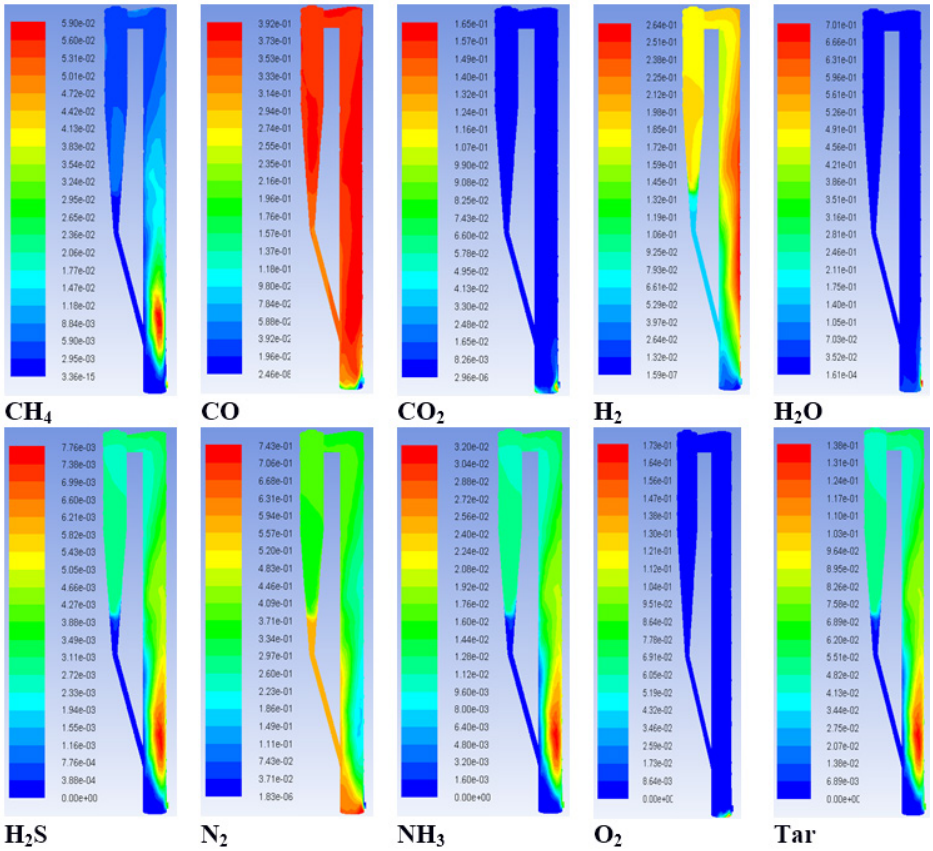

Figure 12. Contours of instantaneous species mole fraction at 10 sec in the CFB gasifier.

reactants fed from the inlet, i.e., O_2 and H_2O are almost completely consumed at or near the inlet and nitrogen in the feed air is almost uniformly distributed in the gasifier.

Contours of CH_4 mole fraction show higher and more uniform concentrations of CH_4 in BFB than in CFB. CO concentration is very high and constant in the CFB. In addition, CO_2 is negligible in the CFB. H_2S and NH_3, which are produced by devolitilization reaction and do not undergo any further reaction, show similar trends in both BFB and CFB. In the case of BFB, higher concentration of these effluents is seen at relatively higher riser height, whereas in ther case of the CFB, it is higher at the production point. The devolitilization reaction seems to elongate in the direction of flow. Tar also shows contours the same as NH_3 and H_2S as oxygen is consumed at the inlet and is not available for oxidation of tar. H_2 is available in both BFB and CFB throughout the gasifier and in approximately the same amounts.

Table 5 shows the composition and temperature of both solid and gas phases. Solid particles are not available at the outlet of BFB, whereas a 3% carbon loss from entrained particles exiting the gasifier is predicted in CFB. The temperature of the solid particles is 1390.32 °C, which is higher than the ash softening temperature. The gas exiting from the CFB is richer in CO and H2 than the gas from BFB. H_2 remains approximately the same, but a major difference can be seen in the concentration of CO and CO_2. CO_2 and CH_4 decreased to a negligible amount and CO approximately doubles when the regime is changed from bubbling to fast fluidization at the same A/C and S/C ratios. Tar content in the gas also decreases.

Table 5. Composition and temperature of gas and solid at the outlet.

	BFB	CFB
H_2O (mol%)	8.76	1.62
O_2 (mol%)	0.0	0.06
N_2 (mol%)	31.44	40.48
CO (mol%)	14.44	35.48
CO_2 (mol%)	11.98	0.46
CH_4 (mol%)	4.90	0.42
H_2 (mol%)	12.71	15.75
NH_3 (mol%)	2.81	1.05
H_2S (mol%)	0.68	0.25
Tar (mol%)	12.26	4.41
Gas Temperature (K)	951.63	1405.31
Char (wt%)		0.03
Volatiles (wt%)		~ 0.0
Moisture (wt%)		~ 0.0
Ash (wt%)		0.97
Solid Temperature (K)		1390.32

CONCLUSIONS

This paper presents a three dimensional full-loop simulation of a circulating fluidized bed gasifier. The model was validated against simulation data. Furthermore, a comparison between bubbling and circulating fluidized bed gasifiers is presented. Keeping temperature, Air/Coal and Steam/Coal constant, hydrodynamic variables such as solid volume fraction, solid axial velocity, gas axial velocity and pressure, along with gasification parameters such as temperature and composition of syngas, are compared. The following conclusions can be drawn from our analysis:

1) In contrast to the BFB, in the CFB the solid particles are distributed throughout the riser, giving rise to more pronounced gas solid contact and in turn better heat and mass transfer will be observed. In addition, in the case of CFB, heterogeneous reactions are not limited to the bed region.

2) In the CFB, a characteristic core-annular flow of solids is observed, whereas BFB shows negative mean axial velocities of solids.

3) In both CFB and BFB, temperature is uniform throughout the riser except near the inlet.

4) In the CFB, A/C = 2.65 is very high as it gives temperatures above the ash softening limit, which is not desirable. Adjustment of the A/C ratio to maintain temperatures below ash softening is required.

5) In the syngas from the CFB, CO (~35%), H_2 (~15%) and N_2 (~40%) are the most prominent gas components, whereas in a BFB, N_2 (~31%) is the most prominent and CO (~14%), CO_2 (~11%) and H_2 (~12%) are present in approximately same amounts at current conditions.

6) When the regime is changed from bubbling to fast fluidization at the same feed temperature and A/C and S/C ratios, H_2 remains approximately the same, CO_2 and CH_4 decrease to a negligible amount and CO approximately doubles. In addition, tar content in the gas also decreases.

REFERENCES

Afrooz, I.E., Sinnathambi, C.M., Karuppanan, S., Ching, D.L.C. CFD Simulation of Bubbling Fluidized Bed: Effect of Distributor Plate Orifice Pattern Configuration on Hydrodynamics of Gas-Solid Mixing. ARPN Journal of Engineering and Applied Sciences, 11, 11954-11959 (2016).

Almuttahar, A., Taghipour, F. Computational Fluid Dynamics of a Circulating Fluidized Bed Under Various Fluidization Conditions. Chemical Engineering Science, 63, 1696-1709 (2008). https://doi.org/10.1016/j.ces.2007.11.020

Armstrong, L.M., Gu, S., Luo, K.H. Parametric Study of Gasification Processes in a BFB Coal Gasifier. Industrial & Engineering Chemistry Research, 50, 5959-5974 (2011). https://doi.org/10.1021/ie1023029

Basu, P. Combustion and Gasification in Fluidized Beds. Taylor Francis, Halifax (2006). https://doi.org/10.1201/9781420005158

Berkowitz, N. An Introduction to Coal Technology. Academic Press, Cambridge (1979).

Bogdanova, V., George, E., Meynet, N., Kara, Y., Barba, A. Numerical CFD Simulations for Optimizing a Biomass Gasifier and Methanation Reactor Design and Operating Conditions. Energy Procedia, 120, 278-285 (2017). https://doi.org/10.1016/j.egypro.2017.07.209

BP, Statistical Review of World Energy. (2017).

Ding, J., Gidaspow, D. A Bubbling Fluidization Model Using Kinetic Theory of Granular Flow. AIChE Journal, 36, 523-538 (1990). https://doi.org/10.1002/aic.690360404

Gidaspow, D., Bezburuah, R., Ding, J. Hydrodynamics of Circulating Fluidized Beds, Kinetic Theory Approach. Proceedings of the 7th Engineering Foundation Conference on Fluidization (Fluidization VII), 75-82 (1992).

Gräbner, M. Industrial Coal Gasification Technologies Covering Baseline and High-Ash Coal. Wiley-VCH, Germany (2015). https://doi.org/10.1002/9783527336913

Gungor, A., Eskin, N. Hydrodynamic modeling of a circulating fluidized bed. Powder Technology, 172, 1-13 (2007). https://doi.org/10.1016/j.powtec.2006.10.035

Gunn, D.J. Transfer of Heat or Mass to Particles in Fixed and Fluidised Beds. International Journal of Heat and Mass Transfer, 21, 467- 476 (1978). https://doi.org/10.1016/0017-9310(78)90080-7

Hassan, M.I.O. Modelling and Simulation of Biomass Gasification in a Circulating Fluidized Bed Reactor, Ph.D. Thesis, Aston University (2013).

Higman, C., van der Burgt, M. Gasification. Gulf Professional Publishing, Amsterdam (2008). https://doi.org/10.1016/B978-0-7506-8528-3.00005-5

IEA, International Energy Outlook. (2017a).

IEA, Energy Access Outlook. (2017b).

Iyengar, R.K., Haque, R. Gasification of High-Ash Indian Coals for Power Generation. Fuel Processing Technology, 27, 247-262 (1991). https://doi.org/10.1016/0378-3820(91)90051-D

Jiang, Y., Qiu, G., Wang, H. Modelling and Experimental Investigation of the Full-Loop Gas-Solid Flow in a Circulating Fluidized Bed with Six Cyclone Separators. Chemical Engineering Science, 109, 85-97 (2014). https://doi.org/10.1016/j.ces.2014.01.029

Johnson P.C., Jackson, R. Frictional-Collisional Constitutive Relations for Granular Materials, with Application to Plane Shearing. Journal of Fluid Mechanics, 176, 67-93 (1987). https://doi.org/10.1017/S0022112087000570

Ju, F., Chen, H., Yang, H., Wang, X., Zhang, S., Liu, D. Experimental Study of a Commercial Circulated Fluidized Bed Coal Gasifier. Fuel Processing Technology, 91, 818-822 (2010). https://doi.org/10.1016/j.fuproc.2009.07.013

Kobayashi, H., Howard, J.B., Sarofim, A.F. Coal Devolatilization at High Temperatures. 18th Symposium (International) on Combustion, The Combustion Institute, Pittsburgh (1977). https://doi.org/10.1016/S0082-0784(77)80341-X

Kraft, S., Kirnbauer, F., Hofbauer, H. CPFD simulations of an industrial-sized dual fluidized bed steam gasification system of biomass with 8 MW fuel input. Applied Energy, 190, 408-420 (2017). https://doi.org/10.1016/j.apenergy.2016.12.113

Li, T., Dietiker, J.-F., Shadle, L. Comparison of Full-Loop and Riser-Only Simulations for a Pilot-Scale Circulating Fluidized Bed Riser. Chemical Engineering Science, 120, 10-21 (2014). https://doi.org/10.1016/j.ces.2014.08.041

Liu, H., Cattolica, R.J., Seiser, R., Liao, C.-H. Three-Dimensional Full-Loop Simulation of a Dual Fluidized-Bed Biomass Gasifier. Applied Energy, 160, 489-501 (2015). https://doi.org/10.1016/j.apenergy.2015.09.065

Liu, H., Cattolica, R.J., Seiser, R. Operating parameter effects on the solids circulation rate in the CFD simulation of a dual fluidized-bed gasification system. Chemical Engineering Science, 169, 235-245 (2017). https://doi.org/10.1016/j.ces.2016.11.040

Liu, H., Cattolica, R.J., Seiser, R. CFD studies on biomass gasification in a pilot-scale dual fluidized-bed system. International Journal of Hydrogen Energy, 41, 11974-11989 (2016). https://doi.org/10.1016/j.ijhydene.2016.04.205

Liu, X., Hu, S., Jiang, Y., Li, J. Extension and Application of Energy-Minimization Multi-Scale (EMMS) Theory for Full-Loop Hydrodynamic Modeling of Complex Gas-Solid Reactors. Chemical Engineering Journal, 278, 492-503 (2015). https://doi.org/10.1016/j.cej.2014.11.093

Loha, C., Chattopadhyay, H., Chatterjee, P.K. Assessment of drag models in simulating bubbling fluidized bed hydrodynamics. Chemical Engineering Science, 75, 400-407 (2012). https://doi.org/10.1016/j.ces.2012.03.044

Lu, B., Zhang, N., Wang, W., Li, J., Chiu, J.H., Kang, S.G. 3D Full-Loop Simulation of an Industrial-Scale Circulating Fluidized-Bed Boiler. AIChE Journal, 59, 1108-1117 (2013). https://doi.org/10.1002/aic.13917

Lun, C.K.K., Savage, S.B., Jeffrey, D.J., Chepurniy, N. Kinetic Theories for Granular Flow: Inelastic Particles in Couette Flow and Slightly Inelastic Particles in a General Flow Field. Journal of Fluid Mechanics, 140, 223-256 (1984). https://doi.org/10.1017/S0022112084000586

Luo, K., Wu, F., Yang, S., Fang, M., Fan, J. High-Fidelity Simulation of the 3-D Full-Loop Gas-Solid Flow Characteristics in the Circulating Fluidized Bed. Chemical Engineering Science, 123, 22-38 (2015). https://doi.org/10.1016/j.ces.2014.10.039

Nikolopoulos, A., Nikolopoulos, N., Charitos, A., Grammelis, P., Kakaras, E., Bidwe, A.R., Varela, G. High-Resolution 3-D Full-Loop Simulation of a CFB Carbonator Cold Model. Chemical Engineering Science, 90, 137-150 (2013). https://doi.org/10.1016/j.ces.2012.12.007

Ogawa, S., Umemura, A., Oshima, N. On the Equation of Fully Fluidized Granular Materials. Zeitschrift für angewandte Mathematik und Physik, 31, 483-493 (1980). https://doi.org/10.1007/BF01590859

Peng, L., Wu, Y., Wang, C., Gao, J., Lan, X. 2.5D CFD simulations of gas-solids flow in cylindrical CFB risers. Powder Technology, 291, 229-243 (2016). https://doi.org/10.1016/j.powtec.2015.12.018

Schaeffer, D.G. Instability in the Evolution Equations Describing Incompressible Granular Flow. Journal of Differential Equations, 66, 19-50 (1987). https://doi.org/10.1016/0022-0396(87)90038-6

Shao, Y., Zhang, Y., Wang, X., Wang, X., Jin, B., Liu, H., Three-Dimensional Full Loop Modeling and Optimization of an in Situ Gasification Chemical Looping Combustion System. Energy Fuels, 31, 13859-13870 (2017). https://doi.org/10.1021/acs.energyfuels.7b02119

Wang, J., Liu, Y. EMMS-based Eulerian simulation on the hydrodynamics of a bubbling fluidized bed with FCC particles. Powder Technology, 197, 241-246 (2010). https://doi.org/10.1016/j.powtec.2009.09.022

Wang, X., Wu, X., Lei, F., Lei, J., Xiao, Y. 3D Full-Loop Simulation and Experimental Verification of Gas-Solid Flow Hydrodynamics in a Dense Circulating Fluidized Bed Particuology, 16, 218-226 (2014). https://doi.org/10.1016/j.partic.2013.11.010

World Energy Council, World Energy Resources: Coal. (2016).

Wu, Y., Liu, D., Ma, J., Chen, X., Three-Dimensional Eulerian−Eulerian Simulation of Coal Combustion under Air Atmosphere in a Circulating Fluidized Bed Combustor. Energy Fuels, 31, 7952-7966 (2017). https://doi.org/10.1021/acs.energyfuels.7b01084

Yan, L., Lim, C.J., Yue, G., He, B., Grace, J.R. Simulation of biomass-steam gasification in fluidized bed reactors: Model setup, comparisons and preliminary predictions. Bioresource Technology, 221, 625-635 (2016). https://doi.org/10.1016/j.biortech.2016.09.089

Yu, X., Blanco, P.H., Makkawi, Y., Bridgwater, A.V. CFD and experimental studies on a circulating fluidised bed reactor for biomass gasification. Chemical Engineering & Processing: Process Intensification, 130, 284-295 (2018). https://doi.org/10.1016/j.cep.2018.06.018

Zhang, H., Huang, W.X., Zhu, J. Gas-solids flow behavior: CFB riser vs. downer. AIChE Journal, 47, 2000-2011 (2001). https://doi.org/10.1002/aic.690470911

Zhang, N., Lu, B., Wang, W., Li, J. Virtual Experimentation Through 3D Full-Loop Simulation of a Circulating Fluidized Bed. Particuology, 6, 529-539 (2008). https://doi.org/10.1016/j.partic.2008.07.013

Zhang, Y., Lei, F., Xiao, Y. Computational fluid dynamics simulation and parametric study of coal gasification in a circulating fluidized bed reactor. Asia-Pacific Journal of Chemical Engineering, 10, 307-317 (2015). https://doi.org/10.1002/apj.1878

Zhao, B., Zhou, Q., Wang, J., Li, J. CFD study of exit effect of high-density CFB risers with EMMS-based two-fluid model. Chemical Engineering Science, 134, 477-488 (2015). https://doi.org/10.1016/j.ces.2015.05.032

Zhou, W., Zhao, C.S., Duan, L.B., Chen, X.P., Liang, C. Two-dimensional computational fluid dynamics simulation of nitrogen and sulfur oxides emissions in a circulating fluidized bed combustor. Chemical Engineering Journal, 173, 564-573 (2011). https://doi.org/10.1016/j.cej.2011.07.083